ADVANCED ELECTRONIC MATERIALS Open Access
www.advelectronicmat.de

Oxygen Defects and Instability in Very Thin a-IGZO TFTs

Hanjun Cho, Masatake Tsuji, Shigenori Ueda, Junghwan Kim, and Hideo Hosono**

Amorphous oxide semiconductor (AOS) thin-film transistors (TFT) have gained significant attention for their potential in capacitor-free next-generation memory applications. However, improving threshold voltage (V_{TH}) stability and precisely controlling carrier concentration in ultra-thin channels remain critical challenges. In this study, an extraordinarily large positive-bias-stress (PBS) instability in hydrogen-free amorphous IGZO (a-IGZO)-TFTs that emerges as the channel thickness decreases is reported. This instability can be attributed to acceptors interacting with donors at shallow levels below the conduction band minimum (CBM). This model, based on temperature-dependent Hall effect measurements, reveals an unusual correlation between donor concentration and donor energy levels. Unlike in previously reported semiconductors, the energy difference between the CBM and donor energy level increases linearly in proportion to (donor concentration)$^{1/3}$. The O 1s core-level hard X-ray photoemission measurements suggest that the entity of the acceptors is oxygen vacancies without two electrons (V_O^{2+}) formed during deposition. These vacancies result from strong donor—acceptor interactions arising from the formation of oxygen Frenkel defects in the thinner films. It is demonstrated that low-temperature extra-annealing effectively suppresses PBS instability by inducing structural relaxation of the Frenkel defects, thereby stabilizing the TFTs.

1. Introduction

Amorphous oxide semiconductors (AOSs) offer significant advantages due to their ease of fabrication at low temperatures, uniform thin-film formation, and the ability to continuously tailor their chemical composition and properties.[1–4] However, the carrier generation mechanism in AOS remains elusive. In amorphous IGZO (a-IGZO), which is widely used as a channel material in thin-film transistors (TFT) for the backplane to drive flat-panel display pixels, defects are present at multiple levels: these include shallow levels below the conduction band minimum (CBM) and deep levels above the valence band maximum (VBM).[5] The precise control of these defects is a significant challenge in the development of amorphous semiconductors. For instance, the performance of TFTs is highly dependent on factors such as high-density hydrogen impurities,[6,7] excess oxygen,[8] and carbon impurities,[9] all of which originate from the fabrication process.

Recently, AOS-TFTs have attracted attention for their potential in next-generation capacitor-free dynamic random access memory (DRAM) applications.[10–16] This interest is driven by their ultra-low off-current of a-IGZO,[17] which is a pivotal for improving retention time in memory devices.[14] However, several obstacles must be overcome to achieve practical implementation. These challenges include the precise control of carrier concentration, threshold voltage (V_{TH}) stability in ultra-thin channels,[18,19] and low contact resistance.[20,21] In this article, we report that (1) the positive-bias-stress (PBS) instability of the V_{TH} in a-IGZO-TFTs significantly increases as the channel becomes very thin, (2) a model for two types of correlations between donor concentration and activation energy, along with supporting evidence, and (3) a proposed solution for improving the stability of very thin channel IGZO-TFTs based on this model. To investigate the mechanisms responsible for this instability, we utilized sputtering to deposit the TFT channels rather than atomic layer deposition (ALD). Although ALD is often used for practical fabrication due to its precise control over film thickness, it can introduce impurity carbon and hydrogen, potentially masking intrinsic phenomena . Addressing these impurities remains a critical challenge in this field, requiring further systematic studies. By employing sputtering under cryo-pumping conditions to reduce impurities of carbon and hydrogen, we aimed to fabricate cleaner TFT channels and reveal the intrinsic behavior of these devices. Understanding intrinsic defects in a-IGZO also provides reference data for addressing fabrication-induced variations in memory devices that employing ALD and complex multi-layer

H. Cho, M. Tsuji, J. Kim, H. Hosono
MDX Research Center for Element Strategy, Institute of Integrated Research
Institute of Science Tokyo
Yokohama 226–8501, Japan
E-mail: tsuji.m.ac@m.titech.ac.jp; hosono.h.aa@m.titech.ac.jp
S. Ueda, H. Hosono
National Institute for Materials Science
Tsukuba, Ibaraki 305-0044, Japan
J. Kim
Graduate School of Semiconductor Materials and Devices Engineering
Ulsan National Institute of Science and Technology
Ulsan 44919, Republic of Korea

The ORCID identification number(s) for the author(s) of this article can be found under https://doi.org/10.1002/aelm.202500349

DOI: 10.1002/aelm.202500349

architectures. Such findings are pivotal to facilitate the oxide memory application. Our novel and unexpected findings suggest that as the channel becomes thinner, the dominant interaction relevant to carrier generation switches from conventional donor–donor interaction to donor–acceptor interaction.

We conducted Hall effect measurements on a-IGZO thin-films as a function of temperature to evaluate the concentration and energy levels of shallow donors. Understanding the relationship between donor density and the energy level with respect to the CBM is crucial for elucidating the carrier generation mechanism. It is well known that the activation energy of donor $E_a(N_D)$ in n-type semiconductors with the donor concentration (N_D) is proportional to $-\alpha(N_D)^{1/3}$, where α is a coefficient.[22–26] Oxide semiconductors reported to date have $\alpha > 0$ to our best knowledge. This implies that an increase in the E_a originates from the electrostatic repulsive interaction between donors because $(N_D)^{-1/3}$ is proportional to the mean separation of defects (d), and Coulomb potential energy is inversely proportional to d. Nevertheless, in our preliminary study of thinner films, we observed the opposite correlation, that is, $\alpha < 0$. This new correlation would come from an attractive interaction between the donor and acceptor. This suggests that donor–acceptor interaction becomes dominant in the thinner film in place of donor–donor interaction. We attribute the responsible acceptor to positively charged oxygen vacancies (V_O^{2+}). A plausible model for V_O^{2+} is the formation of Frenkel defect pairs [V_O^{2+} paired with negatively charged interstitial oxygen (O_i^{2-})] during the deposition process. It is well known that the concentration of Frenkel defect increases with temperature. In the present case, the amorphous structure is frozen from a high-temperature state created by the sputtering process. Thus, the formation of a high concentration of oxygen Frenkel pair is likely to occur in the as-deposited thin a-IGZO thin films. This donor–acceptor model is supported by our experimental results on the O 1s core-level spectra obtained by hard X-ray photoelectron spectroscopy measurement (HAXPES).[27] We propose that extra-annealing at low-temperature can effectively suppress severe PBS instability in very thin a-IGZO TFT by restoring the proposed acceptors, which is experimentally supported by the O 1s core-level spectra obtained by X-ray photoelectron spectroscopy (XPS).

2. TFT Characteristics and Channel Thickness

The effect of channel thickness on V_{TH} was investigated using a bottom-gate and top-contact structure with channels ranging from 5 to 100 nm in thickness. **Figure 1a** shows the transfer curves of fabricated TFTs, indicating that V_{TH} significantly shifts to the positive side as the thickness decreases. Specifically, for a thickness of 100 nm, V_{TH} was − 7.1 V, whereas it was 1.5 V for the 5-nm-thick channel. Since V_{TH} tends to shift negatively with increasing carrier concentration (n_e) in the channel,[9,28] this result is consistent with the Hall effect measurement results summarized in Table S1 (Supporting Information). These results indicate that n_e decreases as the channel becomes thinner. E.g., the n_e was 6.6×10^{16} cm^{-3} for the 100-nm-thick film and 6.0×10^{14} cm^{-3} for the 10-nm-thick film. Figure 1b,d demonstrates that PBS instability becomes more severe as the channel thickness decreases, whereas the negative-bias-stress (NBS) instability shows no distinctive degradation. Figure 1e summarizes the V_{TH} shift after 1 h when channel thickness is varied. The PBS stability tends to degrade significantly for film thicknesses below 50 nm, even when a Zn–Si–O[29] (ZSO, Zn: Si ratio of 70: 30 at.%) capping layer is employed. We used ZSO_x (ZnO-SiO_2) as a passivation layer suitable for a-IGZO channel because it contains Zn which is common in the channel. The amorphous ZSO thin films can be easily deposited at room temperature (RT) by DC sputtering. These features make ZSO favorable for passivation layer of a-IGZO channel. ZSO serves two key functions: (1) effectively blocks impurities from affecting the AOS channel,[9,20,30] and (2) enhances structural relaxation at the thin-film surface and the back-channel by the impact of high energy ions generated during sputtering of ZSO. To investigate whether adsorbed molecules forming surface dipoles on the exposed back-channel[31] contribute to PBS instability, we examined the effect of the ZSO capping layer on the instability of TFTs in the ambient atmosphere. Initially, the device was placed in a vacuum environment (< 1×10^{-4} Pa) to observe V_{TH} stability without applying any bias. Measurements were taken at 2-h intervals over a 12-h period, as shown in Figure S2 (Supporting Information). The results indicate almost no shift in the V_{TH} with ZSO capping, whereas significant instability was observed in the ZSO capping-free TFT. These results suggest that ZSO effectively suppresses the effect of adsorbed molecules, which are a potential cause of PBS instability. The results of a subsequent PBS test with the ZSO capping layer are shown in Figure 1d. Although the large V_{TH} shift (ΔV_{TH} = 3.0 V) by PBS (see Figure 1e) was improved for a 5-nm-thick channel, severe PBS V_{TH} shifts (ΔV_{TH} = 1.6 V) still remained.

These findings suggest that PBS instability arises from two distinct mechanisms: The first is an extrinsic factor, i.e., adsorbed molecules on the surface, which is mitigated by ZSO capping. The second is an intrinsic factor observed in devices with the capping layer, indicating that PBS instability in very thin channels is related to acceptor-type trap states created in bulk. The V_{TH} dependence on channel thickness implies two possibilities: 1) n_e depends on the channel thickness, and 2) very large PBS V_{TH} shifts arise not from surface adsorbed molecules, but rather bulk defects.

3. Correlation between N_D and E_a in a-IGZO Thin-Films

Figure 2a shows the Arrhenius plot of carrier electron concentration (n_e) in a-IGZO thin-films deposited in a different P_{O2}, where thickness is fixed at 100 nm. Both N_D and E_a were calculated by assuming an Arrhenius (thermally activated)-type relationship between temperature and electron carrier concentration (n_e): $n_e = N_D \exp(-E_a/k_B T)$, obtained from Hall effect measurements, where k_B and T are Boltzmann constant and temperature, respectively. As indicated in Figure 2a, the N_D increases and E_a decreases, when P_{O2} during deposition is decreased. Here, we focus on the correlation between N_D and E_a. It is well known that in conventional single-crystalline semiconductors, the E_a decreases as the dopant concentration increases, regardless of conduction type (p or n), as in Si: B, diamond: P, In_2O_3, and GaN: Mg. It is a general consensus in science of amorphous solids that the first neighboring structure such as the coordination number remains even in the amorphous state. Carrier generation occurs from V_O and the local structure around V_O is almost the same as that in

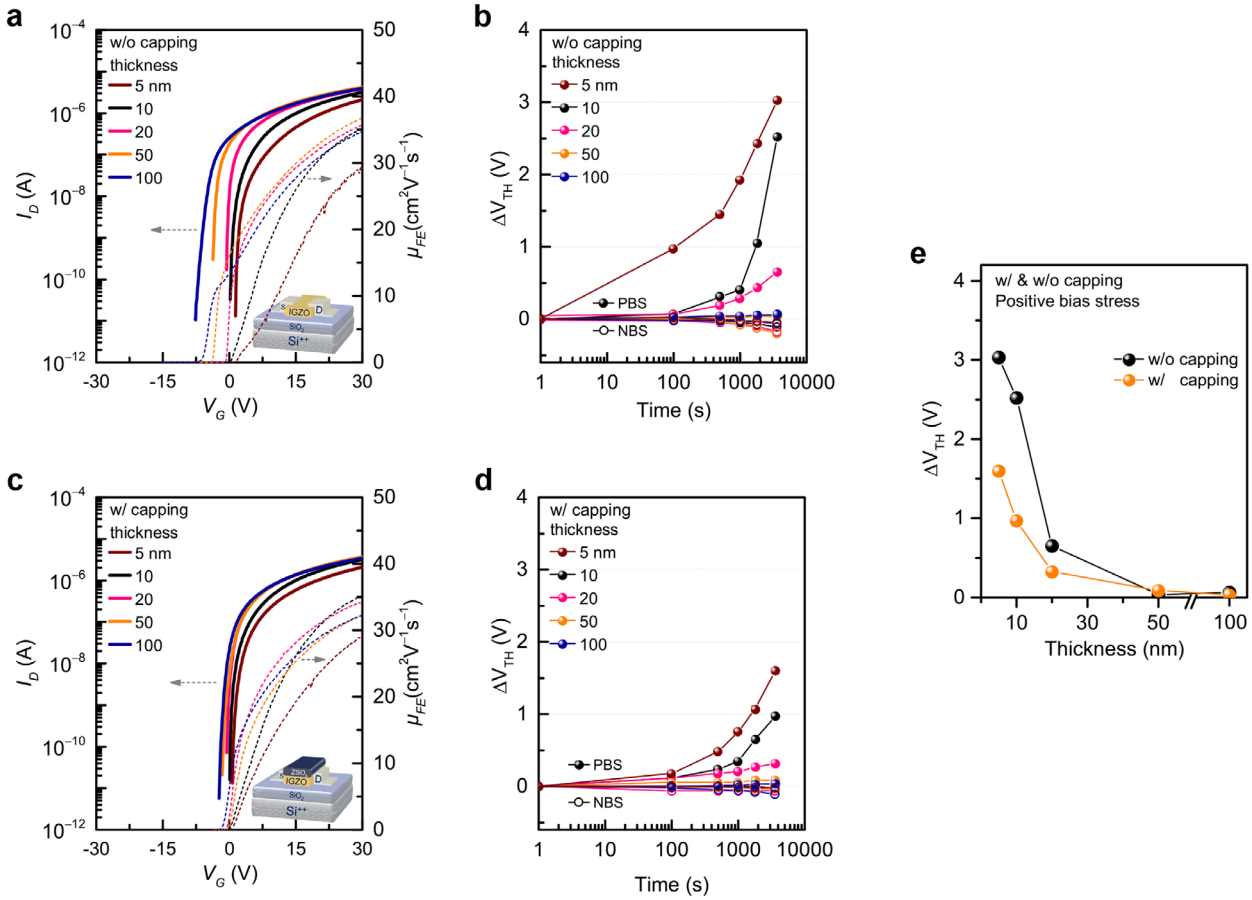

Figure 1. Bias stability of the a-IGZO-TFTs with varying channel thicknesses. Transfer characteristics of a-$In_{0.6}Ga_{0.3}Zn_{0.1}O_x$ (a-IGZO631) TFTs under a partial oxygen pressure of 25% and threshold voltage (V_{TH}) shift as a function of biasing duration a,b) without a capping layer and c,d) with a capping layer, respectively. e) V_{TH} shifts of TFTs with and without a capping layer when channel thickness is varied. The TFT channels were patterned with a width of 60 µm and a length of 30 µm. Transfer curves were acquired with a drain–source voltage of 0.1 V, and a bias of V_{TH} ± 20 V was applied for 1 h in PBS and NBS tests.

crystalline oxide semiconductors. Thus, the empirical relation of $E_a - N_D$ is valid even for an amorphous state. This decrease in E_a with increasing oxygen defect concentration is typically expressed by the empirical equation:

$$E_a\left(N_D\right) = E_a\left(0\right) - \alpha\left(N_D\right)^{1/3} \quad (1)$$

where $E_a(N_D)$ is the energy difference between shallow donors and the CBM, i.e., the E_a of the donor, and $E_a(0)$ is the E_a at a dilute doping limit.[22–26] Note that in this equation, N_D corresponds to the ionized donor concentration rather than the total donor concentration.[26] Again, $(N_D)^{-1/3}$ can relate to the mean separation between the defects (d), where the Coulomb potential energy is inversely proportional to d between charges. As mentioned above, oxide semiconductors exhibit $\alpha > 0$, indicating that the decrease in E_a is due to enhanced interactions between ionized donors. As the N_D increases, the d decreases, leading to stronger repulsive interaction between the donors.[32] As a result, the energy level of the thermally active shallowest donor becomes shallower due to higher potential energy until it reaches a degenerate state that corresponds to $E_a = 0$. Figure 2b shows the correlation between $(N_D)^{1/3}$ and E_a for a-IGZO631. A negative correlation between E_a and N_D is evident; when partial oxygen pressure (P_{O2}) is reduced, N_D increases and E_a decreases, following the relationship described by Equation (1).[27] This result is straightforward to understand that oxygen vacancies (V_O) trapping electrons act as shallow donors in a-IGZO. The energy level of isolated V_O without V_O's interactions, obtained by extrapolating N_D to zero, is E_a = 0.06 eV (see also Figure S3, Supporting Information), which is nearly the same as that of a-IGZO111.[33] This value is close to that (0.09 eV) for single crystalline In_2O_3.[24] As V_O concentration increases by lowering P_{O2}, as shown in **Figure 3a,b**, the d decreases, causing the V_O level to become shallower. The linear relationship between $(N_D)^{1/3}$ and E_a indicates that the interactions between V_O's control the depth of the donor level.

3.1. New Finding of $\alpha < 0$ in the Oxide Semiconductor

Figure 2c shows the Arrhenius plot of n_e in a-IGZO thin-films with different thicknesses (10–100 nm), where P_{O2} is fixed at 25%. The N_D increases and E_a increases, when the thin-film becomes thinner. This trend between E_a and N_D is opposite to that observed in Figure 2a when P_{O2} is varied. It is thus evident that

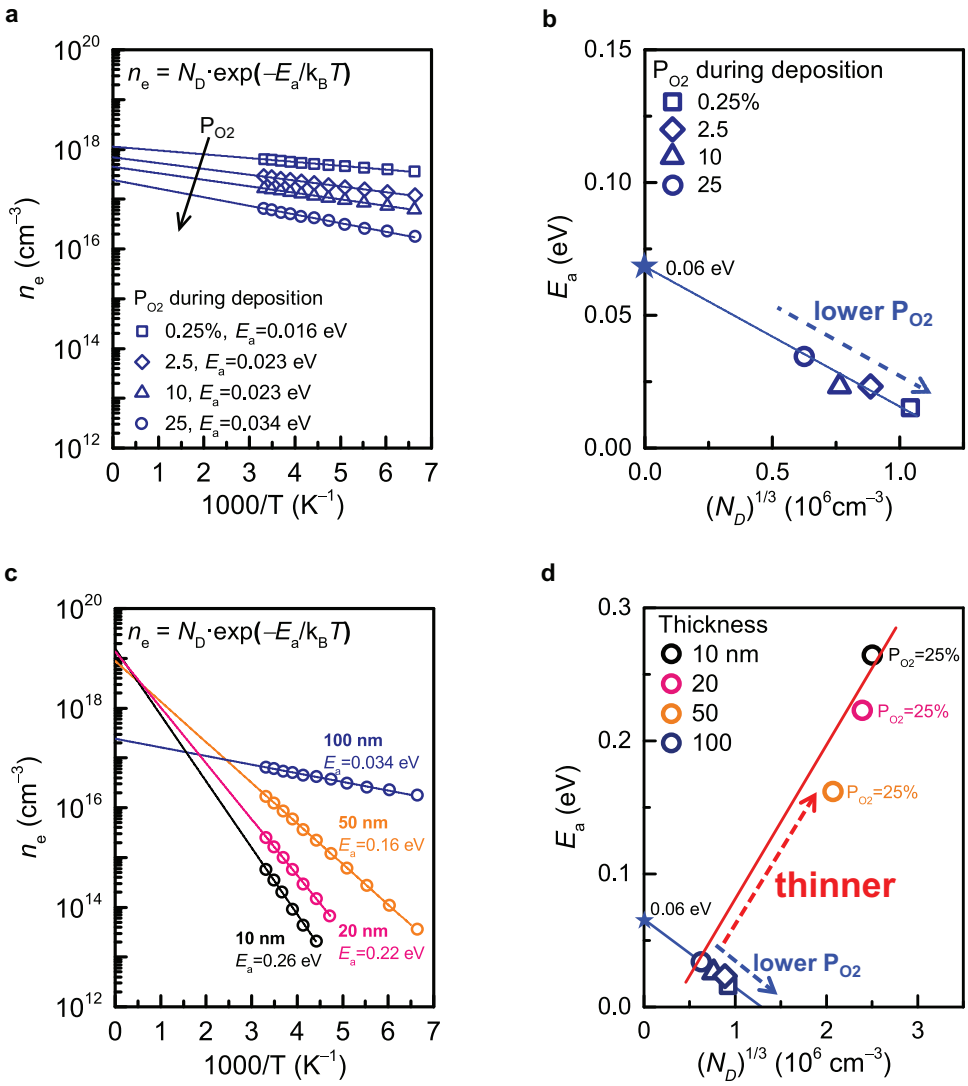

Figure 2. Correlation between donor-level energy (E_a) measured from CBM and donor concentration (N_D) in a-IGZO631. a) The temperature dependence of electron carrier concentration (n_e) in the thin-films when partial O_2 pressure (P_{O2}) is varied during deposition. b) Correlation between $(N_D)^{1/3}$ and E_a when P_{O2} is varied. A star symbol denotes the energy level of oxygen vacancy (V_O) at dilution limit evaluated by extrapolation of N_D to 0. c) The temperature dependence of n_e with varying film thicknesses (10–100 nm). P_{O2} is 25%. d) The correlation between $(N_D)^{1/3}$ and E_a when P_{O2} or thickness is varied. Two opposing types of correlation between $(N_D)^{1/3}$ and E_a are observed: a blue solid line (indicating a negative correlation, or $\alpha > 0$ in Equation 1) and a red solid line (indicating a positive correlation, or $\alpha < 0$ in Equation 1), corresponding to the dependence on P_{O2} and thickness, respectively. The results on $P_{O2} = 0.25\%$ are presented in Figure S4e (Supporting Information), where trends similar to $P_{O2} = 25\%$ are observed.

there are two types of correlation between E_a and N_D. As a-IGZO becomes thinner, a linear relationship ($\alpha < 0$ in Equation 1) between $(N_D)^{1/3}$ and E_a is observed as indicated by the red solid line in Figure 2d. This negative correlation ($\alpha > 0$) switches to the positive correlation ($\alpha < 0$) as the film thickness decreases, even at $P_{O2} = 0.25\%$ (see Figure S4e, Supporting Information), which is a condition that favors the formation of V_O. To explain this positive correlation, an attractive factor for donors is necessary. To date, Equation (1) has been used to explain the decrease in E_a with increasing N_D ($\alpha > 0$) and to analyze the doping effects and electrical properties. Various ideas have been proposed for negative correlation ($\alpha > 0$), including band edge tailing, the attraction between free electrons and positively charged ionized donors,[22] and donor–donor interactions.[32] However, each model explains only for negative correlation ($\alpha > 0$), and does not fully provide a unified interpretation for our findings of both $\alpha > 0$ and $\alpha < 0$. Here, we extend the donor–donor interaction model to defect–defect interactions to explain these observations. We propose the presence of acceptors whose energy levels are located just below the CBM, and the acceptors interact with donors. Namely, as the d decreases, donor–acceptor defect pairs deepen the donor level through attractive interactions, in contrast to donor–donor interactions that induce repulsive effects and lower the activation energy. As a result, donor activation energy increases, as shown in Figure 3c,d. Hereafter, the electronic states of the donor and acceptor are discussed in the ground state at 0 K, which correspond to occupied and unoccupied states, respectively. Following this idea, E_a increases with

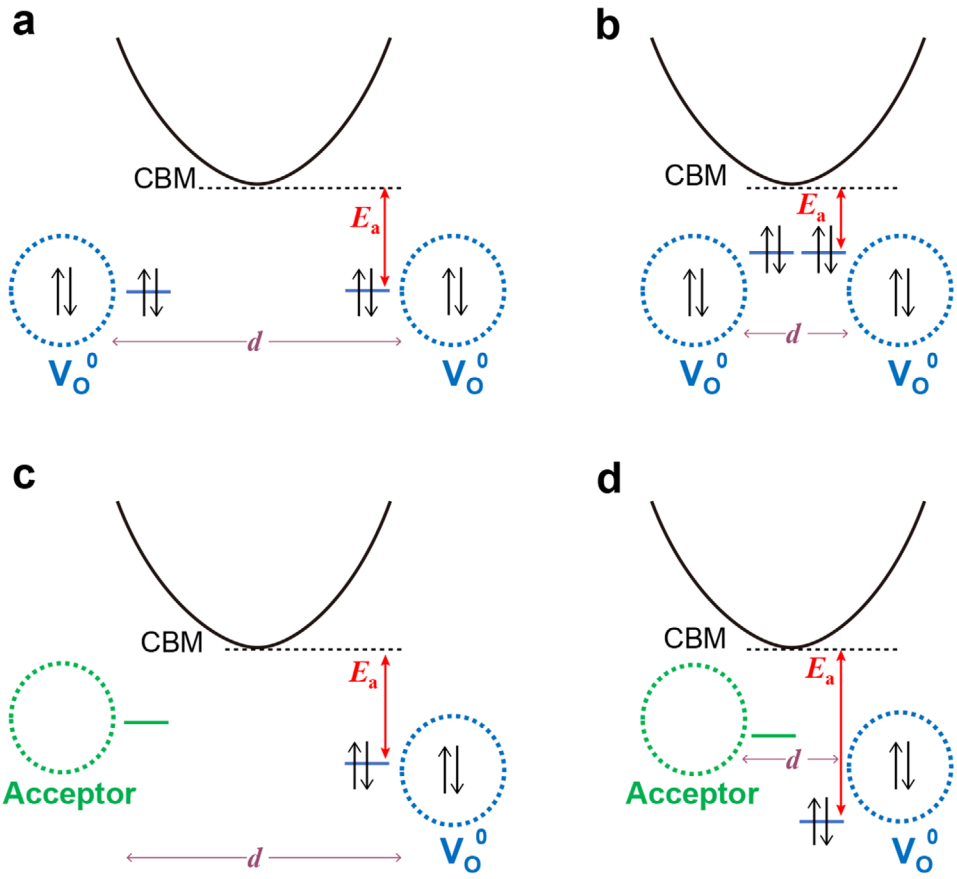

Figure 3. Two types of defect–defect interactions. a,b) Donor–donor repulsive interaction and c,d) donor–acceptor attractive interaction. The effect of change in separation between defects (d) on E_a is schematically illustrated. Note that d is relatively larger in (a,c) than in (b,d).

increasing N_D, in contrast to the case of donor–donor repulsive interaction.

To further understand the correlation between thickness and N_D, we varied the substrate temperature (T_{sub}) during deposition and observed its impact as a function of T_{sub}. The correlation between $(N_D)^{1/3}$ and E_a at T_{sub} during the deposition for a-IGZO111 at $P_{O2} = 0.5\%$ is shown in Figure S5 (Supporting Information). It is evident that N_D decreases as T_{sub} increases, which suggests that structural relaxation during deposition plays a significant role in determining N_D. Most of the defect pairs causing positive correlations are formed during film deposition and are suppressed in part by the structural relaxation owing to substrate heating. Therefore, these defect pairs may be attributed to a metastable state created through a rapid quenching process during deposition. The positive slope shown in Figure 2d can be explained as follows: sputtering deposition occurs by Ar^+ ion-bombardment to the target. Thus, the films grown at low T_{sub} contain a quenched high-temperature state that occurs by ion-bombardment and plasma exposure. Since the equilibrium Frenkel defect concentration increases with temperature, the defect concentration in the as-sputtered thin-film at RT is expected to be high. This rapidly quenched defect state undergoes relaxation during sequential thin-film deposition. As a result, higher defect concentrations remain in the very thin deposited layers.

3.2. What Is the Entity of the Acceptor in a-IGZO?

The next question to address is the entity of the acceptor in a-IGZO. To induce significant defect–defect interactions, small d is necessary for donor–donor interaction, whereas, for donor–acceptor interaction, high concentration of acceptor defects is required. To gain insight into the entity of the acceptor interacting with the donor, we measured the electronic states of thin and thick a-IGZO thin-films by hard X-ray photoemission spectroscopy (HAXPES) in combination with X-ray total reflection (TR).[34,35] **Figure** 4a–c presents the HAXPES spectra in the O-1s region for two samples, one 100-nm-thick (Figure 4a,b) and the other 10 nm (Figure 4c). Figure 4b,c shows the thickness dependence of the O 1s core spectra obtained by surface-sensitive TR-HAXPES (see Note S2, Supporting Information). The main peak is located at around 530 eV and additional peaks appear at a higher binding energy side around ≈531 eV and ≈532 eV. The main peak comes from the oxygen ions bonded with metal cations (In–O, Ga–O, and Zn–O). The sub-peak around 532 eV is attributed to OH in deeper bulk regions.[36–38] The intensity of OH remains unchanged regardless of surface-sensitive (TR-HAXPES), bulk-sensitive (non-TR-HAXPES) measurements, or film thickness, indicating no significant difference is seen between the thin and thick films. A notable difference between the thin (10 nm) and thick (100 nm) films is the intensity of the peak

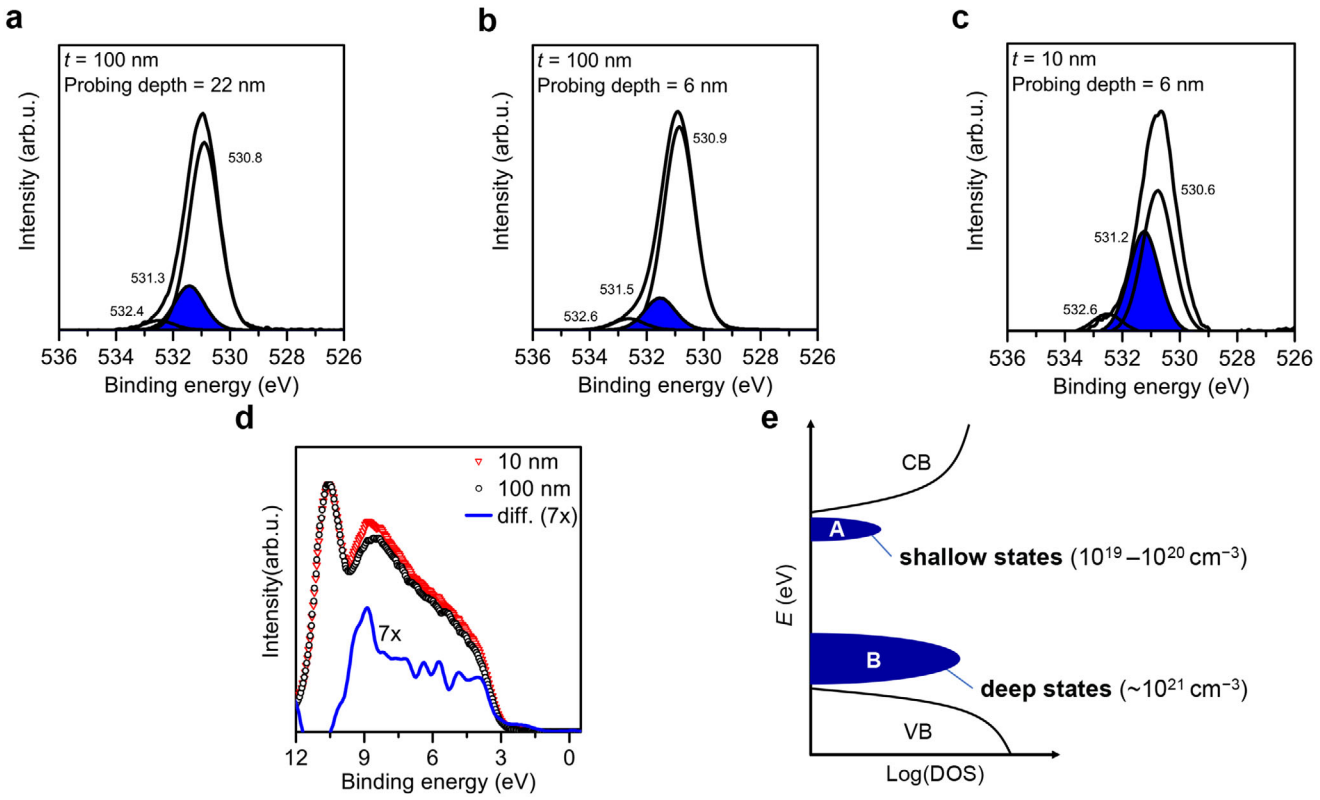

Figure 4. HAXPES spectra of a-IGZO111. a–c) O 1s core-level HAXPES spectra for a,b) 100-nm-thick and c) 10-nm-thick a-IGZO111 films. HAXPES combined with X-ray total reflection (TR-HAXPES) was used to obtain the spectra in (b) and (c). The O 1s peaks are deconvoluted into three components. d) Valence band (VB) TR-HAXPES spectra of 10- and 100-nm-thick films and the difference spectrum between them. The photon energy was set to 5.95 keV. e) Simplified schematic of the experimentally clarified density of states (DOS) of two types of oxygen vacancies in a-IGZO.

at ≈531 eV relative to the main peak at ≈530 eV.[27] This observation suggests the presence of oxygen species that are weakly bound than lattice O^{2-}.[39] The origin of the O 1s peak components located at ≈531–532 eV in oxide semiconductors looks rather confusing. While not a few studies describe these peaks as an oxygen vacancy (so-called "V_O"),[37,40] V_O has no electron in the core-level region, in principle. This means that V_O itself should not directly give any peak in the O 1s core-level region. Here, we propose a plausible model that the O 1s peak at ≈531 eV is attributed to oxygen perturbed by the interstitial oxygen suggested in Refs.[41–43] This interstitial oxygen (O_i) leads to the formation of the acceptor, namely V_O^{2+} (an oxygen vacancy without two electrons), which interacts with V_O^0 (an oxygen vacancy with two electrons). An origin for this donor–acceptor interaction would be the formation of Frenkel defect pairs. The concept of Frenkel pairs in ionic solids is well-established and is observed even in amorphous materials because the local structure in crystal remains even in the amorphous state. The clear formation of Frenkel defect was observed in a-SiO_2.[44–46] According to this "oxygens perturbed by O Frenkel defect" model, a comparison between the 10- and 100-nm-thick a-IGZO thin-films in Figure 4b,c reveals that the intensity of so-called "V_O" relative to that of the lattice O^{2-} is distinctly larger in the thinner (10 nm) film than in the 100-nm-thick film.

The observed difference in the chemical state of oxygen is expected to affect the DOS of the VB. Figure 4d shows the VB TR-HAXPES spectra of the 10- and 100-nm-thick films, normalized by the intensity of Zn 3d core-level located at ≈10.5 eV. The intensity difference spectrum shows the finite intensity, which is slightly enhanced in the 10-nm-thick film and is mainly composed of O 2p orbitals in the entire VB region. The enhanced intensity is attributed to the perturbed oxygen, which correlates with the O 1s peak (so-called "Vo") at ≈531 eV in Figure 4b,c. A possible explanation for the difference between the thick and thin a-IGZO is the enhancement of oxygen-related defects in the thinner films, such as interstitial oxygen (O_i),[8] O_2^-, or O_2^{2-}. Among them, O_i and O_2^{2-} are more likely than O_2^- because no EPR signal was observed (data not shown here), notwithstanding O_2^- is paramagnetic. Figure S7c (Supporting Information) presents thermal desorption spectra (TDS) of m/Z = 32 (O_2) from a-IGZO111 films. Desorption of O_2 from the thin-films was not observed; thus, the possibility of excess oxygen being incorporated into the thin-films during deposition is unlikely. The observed results suggest the formation of interstitial oxygen species in stoichiometry by the Frenkel defect mechanism.

Figure 4e illustrates that oxygen vacancies (V_O) can be categorized into two types: deep states and shallow states. The deep states above the VB are observed by HAXPES, while the information on the shallow states is obtained from temperature-dependent Hall effect measurements. We consider the distinction between deep and shallow states lies in the size of the oxygen vacancy site based on molecular dynamics (MD) simulation:[47]

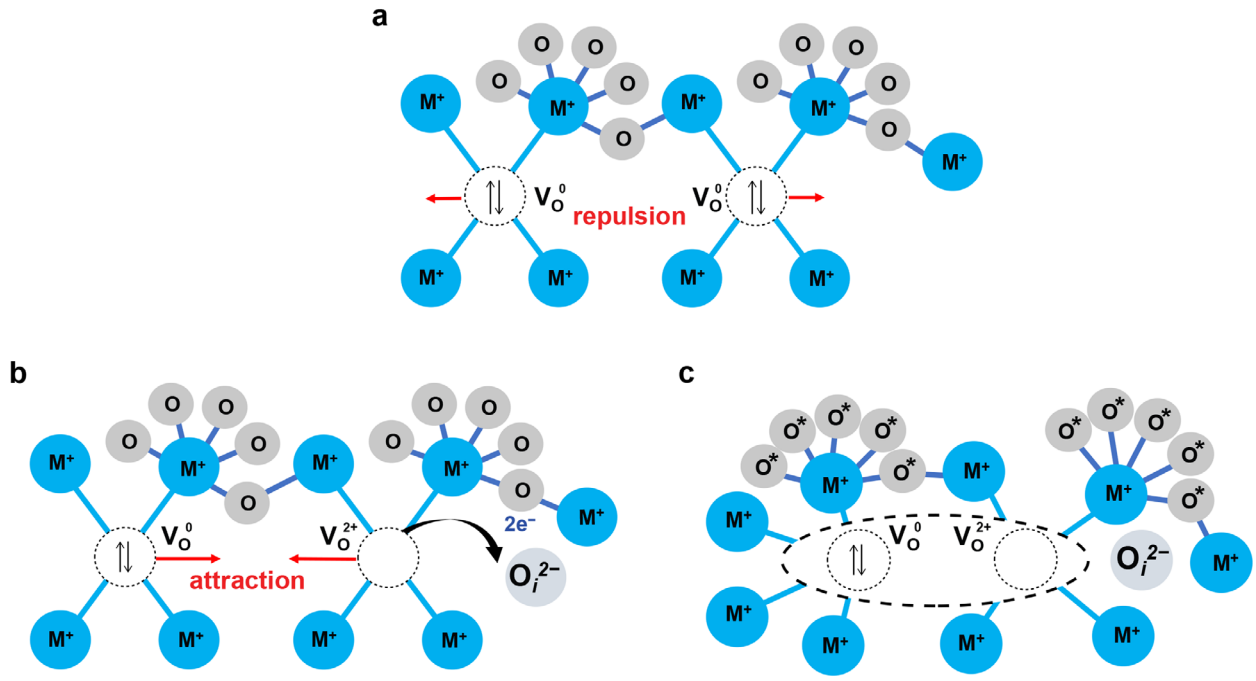

Figure 5. A schematic model for two types of defect–defect interactions. a) A donor–donor interaction is dominant, and the responsible defect is Vo trapping 2 electrons, originated from oxygen deficiency. b) Distortion of lattice oxygen in a-IGZO, leading to the formation of a Frenkel-type defect pair. c) Relaxed structure of a-IGZO with a V_O^{2+}–O_i^{2-} pair, which may be regarded as Frenkel defect. In practice, these defects may be led by bond angle distortion in metal-oxygen octahedra (MO_6). Namely, the second-neighboring oxygen, perturbed by V_O^{2+}–O_i^{2-} pair (denoted as O*), is a plausible candidate responsible for the O 1s peak located at ≈531 eV, so-called "V_O" detected by XPS.

larger space forms an electron trap level deep in the band gap, otherwise, smaller space is necessary to form shallow states. There is a variety of sub-gap states in a-IGZO from multiple sizes around oxygen vacancy according to the MD simulation.[48] G.W. Mattson et al. reported that hydrogen incorporation creates a broad distribution of electronic states in mid-gap.[7] Here, we emphasize that our thin films are hydrogen-free a-IGZO, with hydrogen contamination below the TDS detection limit (≈10^{18} cm^{-3}) before and after annealing, respectively. For simplicity, we categorize these states as shallow and deep states, with both states detected in the O 1s core-level HAXPES spectra through perturbed oxygen. Notably, the deep states are quantitatively dominant, being 1–2 orders of magnitude larger than the shallow states.

3.3. Interstitial Oxygen and Oxygen Vacancy Pair

According to calculations[49–52] on defects in relevant oxides, interstitial oxygen (O_i) forms unoccupied states just below the CBM depending on the chemical composition. In β-Ga_2O_3 and In_2O_3, the O_i and lattice oxygen are closer together to form energetically stable molecular oxygen. Comparisons of the defect formation energies assumed for In, Zn-rich, and Ga-rich IGZO are summarized in Figure S8 (Supporting Information). The preferentially formed interstitial oxygen-related defects depend on the chemical composition: in In-rich a-IGZO, Fermi-level (E_F) is pinned by V_O and O_i, resulting in the formation of molecular oxygen. In contrast, in Ga-rich a-IGZO, O_i itself can be stabilized. It is important to note that these electronically active oxygen species would typically be deactivated by competition with hydrogen-related impurities. In this study, we suppose that the intrinsic defect in a-IGZO was observed because the concentration of hydrogen impurities was below the detection limit of TDS (≈10^{18} cm^{-3}) for the as-deposited thin-films. The hydrogen impurity concentration in this work is two to three orders of magnitude lower than that previously reported in conventional sputtering under turbo-molecular-pumping, which contains impurities of carbon and hydrogen.[53]

Figure 5a–c illustrates two types of defect–defect interaction models. In the conventional a-IGZO case, as reported in previous studies,[5] the formation of oxygen vacancies (V_O^0) trapping two electrons originated from oxygen deficiency is depicted in Figure 5a. For the donor–acceptor interaction in Figure 5b,c, V_O^{2+} is formed by distortion of lattice oxygen in a-IGZO (Figure 5b), especially in the very thin films. Furthermore, the V_O^{2+}–O_i^{2-} pair, which may be regarded as Frenkel defects (Figure 5c), leads to the formation of large vacancy sites that may explain the origin of deep states.

The following is a rough estimate of the concentration of oxygen perturbed by the V_O^{2+}–O_i^{2-} pair. On the assumption that the oxygen constituting a point-shared MO_6 octahedron with a distorted bond angle is perturbed by the oxygen Frenkel defect pair, the number of second-neighboring oxygen (O*) can be expressed as:

$$\text{Number of } O^* = 2 \times (\#\text{ of distorted } MO_6 \text{ octahedron}) \times (CN - 1) \quad (2)$$

where *CN* is the coordination number around the cation adjacent to V_O. In the case of a-IGZO, the estimated number of O* around the Frenkel defect is ≈40. Since the N_D for a-IGZO111 film is ≈1×10^{20} cm^{-3} for thinner film (Figure S4, Supporting Information), the O* concentration in the thin-film is ≈4×10^{21} cm^{-3}. By comparison, the concentration calculated from the area of the XPS O 1s peak at 531 eV is in the range of 5×10^{21} to 1.5×10^{22} cm^{-3}, corresponding to 10–30% of the total O^{2-}. The comparable values of the XPS-derived concentration and the estimated concentration of perturbed oxygen (O*) support this idea that the second-neighboring oxygen, perturbed by the V_O^{2+}–O_i^{2-} defect pair, is responsible for the O 1s peak located at ≈531 eV. During TFT operation, the proposed acceptor (V_O^{2+}) may act as a carrier trap and deteriorate ON characteristics, resulting in a positive V_{TH} shift. In other words, even with the same n_e, the film thickness significantly affects the stability of the TFT operation.

4. Improved PBS Stability in Very Thin a-IGZO TFT

These results indicate that both the fabrication conditions, such as P_{O2} and thickness, and the chemical composition of a-IGZO must be carefully considered to have improved TFT stability. It is known that increasing the Ga concentration reduces the n_e in a-IGZO.[2,54] The previous analysis focused solely on n_e without considering E_a or N_D. Here, we employed temperature-dependent Hall measurements to determine N_D and E_a, as shown in **Figure 6a**. Notably, the E_a values strongly depend on the chemical composition, and decreasing the In/Ga ratio does not necessarily reduce the oxygen defect concentration (N_D). Instead, higher Ga content to In leads to deepens the donor levels, which explains the observed decrease in n_e. The trends in E_a as a function of $(N_D)^{1/3}$ for the different In/Ga ratios in a-IGZO are summarized in Figure S4 (Supporting Information). Figure 6b illustrates the relationship between $(N_D)^{1/3}$ and E_a under different fabrication conditions, such as P_{O2}, film thickness, and the chemical composition of a-IGZO. A negative correlation (blue dashed arrow in Figure 6b) is observed with increasing film thickness, decreasing P_{O2}, or increasing the In/Ga ratio, indicating enhanced donor–donor interaction. Conversely, a positive correlation (red dashed arrow in Figure 6b) is observed as the thickness decreases (see also Figure S4e,f), suggesting that donor–acceptor interaction becomes dominant. Additionally, as the P_{O2} increases or the In/Ga ratio decreases (red dashed arrow in Figure 6b), the concentration of Vo^0 (oxygen vacancies with two electrons) decreases, leading to a reduced contribution from donor (Vo^0)–donor (Vo^0) interactions. As a result, the donor (Vo^0)–acceptor (Vo^{2+}) interaction becomes apparent. Based on these observations, we can identify two origins for the formation of "oxygen defects": i) the oxygen-deficient type, which is commonly known, Vo^0 (with 2 electrons), formed in off-stoichiometric oxide semiconductors for transparent conductive oxides (TCOs), and ii) intrinsic V_O^0, which forms as the Frenkel defect during deposition, even in stoichiometric and hydrogen-free a-IGZO thin-films.

Figure 6c summarizes the dominant defect–defect interactions and their impact on TFT instability in the E_a–$(N_D)^{1/3}$ diagram. Three types of oxygen-related defects influence electron transport properties: (i) V_O^0, caused by oxygen deficiency, which can be categorized into deep and shallow states, with the shallow states affecting electron transport properties; (ii) O_i^{2-}; and (iii) V_O^{2+}, located just below the CBM, acting as a gate-bias-dependent acceptor. A reduction in Frenkel defects (V_O^{2+}–O_i^{2-}) leads to the dominance of donor (V_O^0), resulting in deteriorated NBS instability. Conversely, an increase in Frenkel defects causes acceptor (V_O^{2+}) to become dominant, leading to deteriorated PBS instability. Viewing the diagram with the above-consideration helps explain the extraordinarily large PBS instability observed in very thin a-IGZO TFTs and highlights the existence of a "sweet spot" for AOS-TFTs, where the device is least affected by NBS and/or PBS instability. This optimal condition can be achieved by increasing the AOS thickness, adjusting the In/Ga ratio, or reducing P_{O2} during deposition. Conversely, for TFTs prone to NBS instability due to dominant donor–donor interactions, reducing the AOS thickness, decreasing the In/Ga ratio, or increasing the P_{O2} during deposition may be necessary to reach the sweet spot by suppression of donor formation. Understanding these dominant defect interactions and fine-tuning fabrication conditions are crucial for successfully producing high-performance TFTs. By identifying these factors, the performance and reliability of devices can be enhanced, ensuring that the devices are tailored to withstand specific stress conditions. Furthermore, the negative and positive correlations between $(N_D)^{1/3}$ and E_a in Figure 6c provide insight into the fundamental differences between transparent oxide semiconductors and TCOs. TCOs such as Sn-doped In_2O_3, F-doped SnO_2, and Al-doped ZnO require high electrical conductivity like metals.[55] Therefore, increasing N_D with decreasing E_a (i.e., negative correlation) is typically desirable for TCOs.

Historically, AOS-TFTs with thick channels have been susceptible to NBS instability due to the dominance of donor–donor interactions. However, as the channel thickness decreases to 10 nm or less, oxygen-related acceptors, such as Frenkel defects, become traps, making PBS instability more prominent. To address the serious PBS instability caused by Frenkel defects in very thin a-IGZO, it was necessary to reduce the acceptor concentration. We modified the conventional thin-film process by introducing an additional low-temperature annealing step after deposition. The process began with a 400 °C post-deposition thermal annealing in air for 1 h. After cooling to RT, the samples underwent an additional low-temperature thermal annealing at 200 °C in air for 1 h. As a result, we observed a noticeable decrease in N_D and E_a, indicating a reduction in the concentration of donor–acceptor pairs, as illustrated in Figure 6d. It is important to note that the initial thermal annealing and the extra-annealing serve different roles and operate via different mechanisms. The first annealing cycle, involving heating and cooling (known as the post-annealing process) above 300 °C, is well known for improving TFT performance, stability, and uniformity.[5,56,57] It is reported that the densification is observed to occur ≈1% around 400 °C as a result of macro-relaxation.[58] This process was suitable for the elimination of defects and voids so far. However, temperatures above 300 °C are too high to restore Frenkel defects to regular M–O–M bonds. On the other hand, low-temperature annealing below 300 °C has been reported to reduce tail-state optical absorption while preserving the amorphous structure without detectable densification.[58] Therefore, additional low-temperature thermal annealing at around 150–250 °C is necessary to stabilize oxygen species.

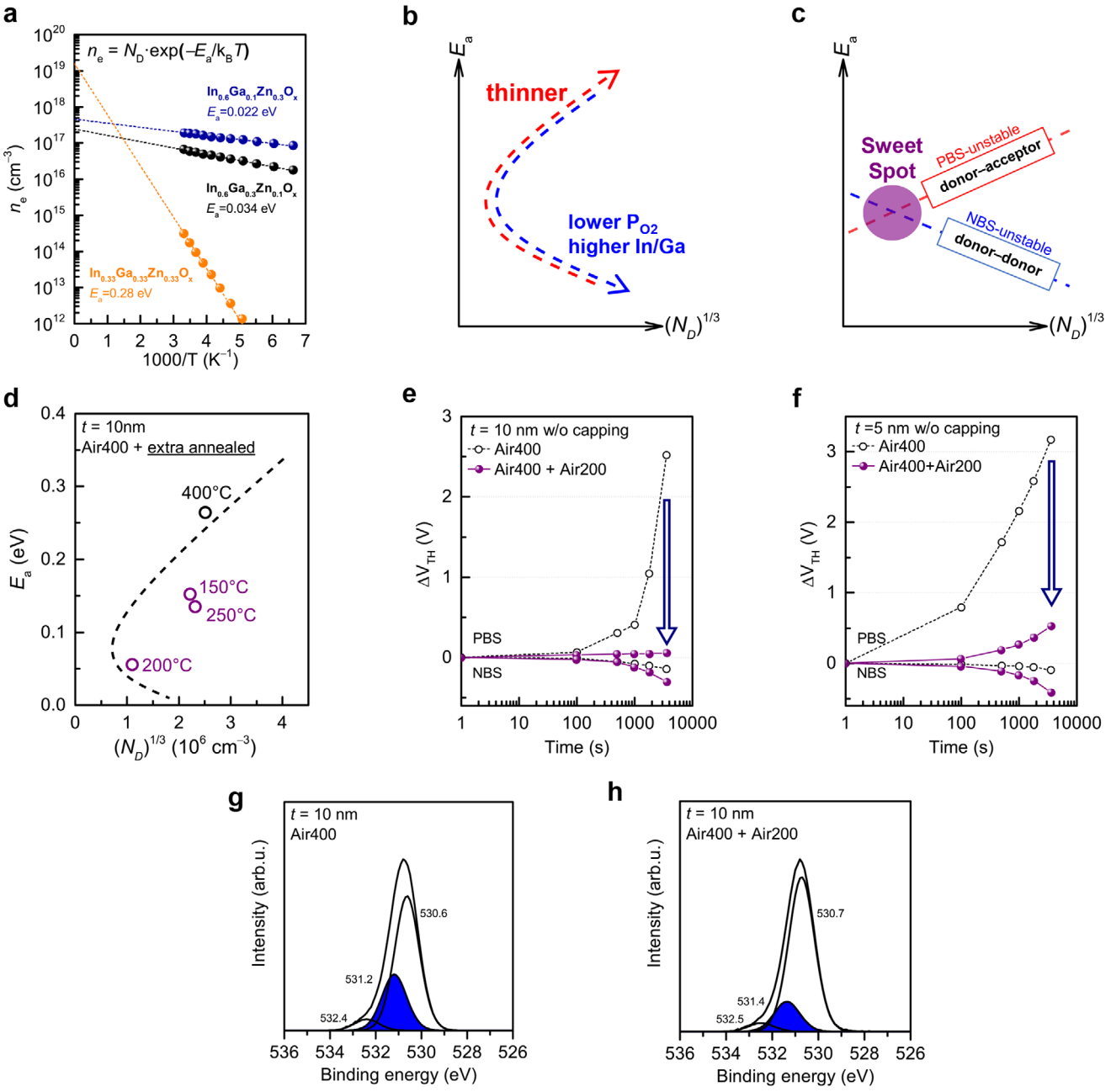

Figure 6. Improved TFTs stability through low-temperature extra-annealing. a) Temperature dependence of the n_e in a-$In_{0.33}Ga_{0.33}Zn_{0.33}O_x$ (a-IGZO111), a-$In_{0.6}Ga_{0.3}Zn_{0.1}O_x$ (a-IGZO631), and a-$In_{0.6}Ga_{0.1}Zn_{0.3}O_x$ (a-IGZO613). b) Correlation between $(N_D)^{1/3}$ and E_a with deposition conditions; P_{O2}, film thickness, and chemical composition. Depending on the fabrication conditions, correlations switch from negative to positive (red dashed arrow) or from positive to negative (blue dashed arrow). c) Schematic relationship between two types of correlation and PBS/NBS instabilities in an E_a–$(N_D)^{1/3}$ diagram. The purple area indicates the optimal N_D and E_a region for NBS/PBS-stable TFTs. d–f) Extra-annealing effect on transfer TFT characteristics. To achieve a high-mobility, ultra-thin TFT with a-IGZO631 channel was employed. d) N_D and E_a after extra-annealing at various temperatures. Results of bias stability tests of 200 °C extra-annealed a-IGZO631 TFTs with e) 10-nm-thick and f) 5-nm-thick active layers. For PBS and NBS tests, a positive or negative bias of V_{TH} ± 20 V was applied with a V_{DS} of 0.1 V. g, h) Extra-annealing effect on the O 1s core-level XPS spectra in 10-nm-thick a-IGZO111 films. g) 400 °C-1 h annealed thin-film; h) thin-film after 200 °C-1 h extra-annealing.

Figure 6e,f demonstrates the improved characteristics of the 10-nm-thick and 5-nm-thick TFT channels after undergoing low-temperature extra-annealing at 200 °C. The concentration of oxygen-related acceptors decreased as the oxygen became more stable due to the annealing process. This stabilization led to the thermal restoration of the oxygen-related acceptors, resulting in an increase in n_e and a negative shift in V_{TH} from 0.2 V to −4.5 V for the 10-nm-thick TFT channel and 0.4 V to −2.5 V for the 5-nm-thick TFT channel (see Figure S11, Supporting Information). Additionally, the extraordinarily large PBS V_{TH} shift was

significantly reduced from 2.5 V to 0.06 V for 10-nm-thick and 3.2 V to 0.5 V for 5-nm-thick, as shown in Figure 6e,f. The remaining PBS V_{TH} shift (0.5 V) in the 5 nm-thick TFT may be attributed to surface effects such as adsorption of molecules. For TFTs with a channel thickness of less than 10 nm, further investigation is required to optimize the chemical composition and fabrication conditions. However, there was a minor degradation in NBS performance, which can be attributed to the shift in the dominant interaction from donor–acceptor to donor–donor after extra-annealing, making the donor–donor interaction more prominent when the gate bias is applied. To further understand how low-temperature extra-annealing restores Frenkel defects, we measured the electronic states of very thin a-IGZO111 films using conventional XPS using Al Kα light source (1486.7 eV). Figure 6g,h shows the O 1s core-level XPS spectra for two films: one annealed at 400 °C (Figure 6g) and the other subjected to an additional low-temperature annealing at 200 °C (Figure 6h). Notably, there is a clear reduction in O 1s peak intensity at ≈531 eV. These results suggest that the concentration of oxygen-related acceptors occupying interstitial sites decreases by extra-annealing, leading to a reduction in donor–acceptor pairs.

5. Conclusions

The primary points of the present paper are summarized as follows:

I. An extraordinarily large PBS instability was observed in hydrogen-free a-IGZO thin films (≈5 nm) deposited by sputtering, and its mechanism was elucidated. The instability was caused by insufficient n_e due to donor level deepening from donor–acceptor interactions at V_G = 0 V and carrier trapping by acceptors under positive V_G.
II. Two types of correlations between N_D and E_a in a-IGZO were identified, and the opposite E_a shifts with N_D were explained by interactions between defects. In the very thin films, high-concentration donor–acceptor pairs increase E_a with N_D, suppressing n_e. The dominant correlation is determined by fabrication conditions, such as film thickness, deposition P_{O2}, and the In/Ga ratio, which control dominant defect–defect interactions and indicate whether the V_{TH} shift is more prone to NBS or PBS instability.
III. The presence of oxygen-related acceptors is suggested by HAXPES measurements on the VB and O 1s. These TFT and HAXPES measurements revealed that high concentrations of V_O^0 (as the donor) and V_O^{2+} (as the acceptor) were formed in thinner a-IGZO films. The V_O^{2+}–O_i^{2-} pair may be regarded as a Frenkel defect and V_O^{2+} can act as a gate-bias-dependent acceptor and was identified as a plausible origin of the PBS instability.
IV. Low-temperature extra-annealing was demonstrated to be effective to restore oxygen-related acceptor defects, allowing the fabrication of very thin a-IGZO TFTs with high stability.
V. A plausible structural model for so-called "V_O" component in O 1s XPS spectra was proposed.

This study provides a pathway for developing high-bias-stability a-IGZO TFT devices with very thin channels by combining precise control of defect interactions through fabrication tuning and the implementation of low-temperature extra-annealing.

6. Experimental Section

Thin-Film Deposition and Hall Effect Measurement: To compare donor-level and concentration characteristics across varying carrier concentrations and chemical compositions, three different indium/gallium (In/Ga) ratios were prepared: a-$In_{0.33}Ga_{0.33}Zn_{0.33}O_x$ (a-IGZO111), a-$In_{0.6}Ga_{0.3}Zn_{0.1}O_x$ (a-IGZO631), and a-$In_{0.6}Ga_{0.1}Zn_{0.3}O_x$ (a-IGZO613). These films, ranging from 10 to 100 nm in thickness, were deposited using RF magnetron sputtering without intentional heating. The sputtering conditions were as follows: RF power of 150 W, 3-inch diameter targets, total pressure of 0.4 Pa, and back-pressure of the deposition chamber of ≈2×10^{-7} Pa, achieved using cryo-pumping. The partial oxygen pressure (P_{O2}) was varied between 0.25–25%, corresponding to the limits of stable plasma generation under oxygen-poor and oxygen-rich conditions. After the deposition, the samples were annealed at 400 °C for 1 h in ambient air. For ohmic contacts, Mo (80 nm) electrodes were sputtered through a shadow mask for a-IGZO111, and Au (80 nm) electrodes were used for a-IGZO631 and a-IGZO613. It should be noted that the measurement of carrier concentration for thin-films thinner than 10 nm was not feasible due to the detection limit.

TFT Device Fabrication: To achieve a high-mobility, ultra-thin TFT, a-IGZO631 was employed in the fabrication of bottom-gate and top-contact TFT structures. P^{++}-silicon substrates were used, featuring a 150 nm thermally grown SiO_2 gate insulator. The a-IGZO631 films, ranging from 5 to 100 nm in thickness, were deposited via RF magnetron sputtering without intentional heating. The sputtering parameters were as follows: RF power of 150 W, 3-inch diameter target, total pressure of 0.4 Pa, and back-pressure of ≈2×10^{-7} Pa, with a P_{O2} of 25%. Post-deposition heat treatment was conducted under the same conditions as described above. The TFT channels were patterned with a width of 60 µm and a length of 30 µm by photolithography (MA-10, Mikasa). Following this, conductive Mo (10 nm) and Au (70 nm) were deposited as the source/drain electrodes. Additionally, a 5-nm-thick amorphous Zn–Si–O[9,20,29,30] (ZSO) capping layer, with a Zn: Si ratio of 70:30 at.%, was deposited under a total pressure of 0.4 Pa, back-pressure of ≈2×10^{-7} Pa and P_{O2} of 25%.

Samples for Hard X-Ray Photoelectron Spectroscopy (HAXPES) Measurement: To facilitate HAXPES measurements, 10-nm- and 100-nm-thick a-IGZO111 films were prepared, using the standard a-IGZO chemical composition. Due to the limitations of Hall measurements at 5-nm thickness, data consistency could not be verified for such thin-films. For these samples, Conductive Ti (10 nm) and Pt (50 nm) layers were deposited onto silicon substrates. The substrates underwent thermal annealing at 800 °C for 1 h in a vacuum to remove adsorbed molecules. Subsequently, a-IGZO111 films were deposited via RF magnetron sputtering without intentional heating, using the following sputtering parameters: RF power of 150 W, 3-inch diameter target, total pressure of 0.4 Pa, back-pressure of ≈2×10^{-7} Pa, and P_{O2} of 0.25%. After deposition, the samples were annealed under the same conditions as previously described.

Characterization of Devices and Thin-Films: The film thickness was measured using grazing-incidence X-ray reflectivity spectroscopy (SmartLab, Rigaku). The presence of oxygen molecules in a-IGZO thin-films was evaluated by thermal desorption spectroscopy (TDS, ESCO). Carrier transport properties of the a-IGZO thin-films were investigated through AC magnetic field Hall effect measurement (ResiTest8400, TOYO) with the van der Pauw configuration, under an AC magnetic field of 0.4 T at 300–150 K in a helium atmosphere (Note S1, Supporting Information). Depth-dependent electronic structures were measured using hard X-ray photoemission spectroscopy (HAXPES) in combination with X-ray TR[34,35] for the 100- and 10-nm thick a-IGZO films at RT at the undulator beamline BL09XU[59] of SPring-8 (Note S2, Supporting Information). The electronic structures for the 10-nm-thick a-IGZO films were also analyzed by conventional X-ray photoemission spectroscopy (XPS) using Al Kα radiation ($h\nu$ = 1486.6 eV) (Note S2, Supporting Information). Ar^+ ion sputtering was

performed to remove surface contamination from carbon and hydroxyl groups (Figure S9, Supporting Information).

Supporting Information

Supporting Information is available from the Wiley Online Library or from the author.

Acknowledgements

H.C. and M.T. contributed equally to this work. H.H. conceived and supervised the research. H.C., M.T., and J.K. conducted the experiments. H.C., M.T., and S.U. performed the HAXPES measurements. All the authors contributed to the discussion on the results and mechanism. H.C., M.T., and H.H. wrote the manuscript mainly. All the authors have given their approval to the final version of the manuscript. The authors thank Minoru Tazoe and Yukiko Sato for their experimental assistance, and Michiko Sato for XPS measurements. The HAXPES measurements were performed with the approval of JASRI/SPring-8 (Proposals 2023A1572, 2023A1720, and 2023A1917). The authors thank Akira Yasui for technical assistance in the HAXPES experiments. This work was partly supported by the MEXT Program: Data Creation and Utilization Type Material Research and Development Project (Grant No. JPMXP1122683430). M.T. was supported by KAKENHI (Grant Numbers JP23K19266 and JP24K17753). This work was partly supported by Samsung Electronics Co., Ltd (Grant No. IO240217-09010-01).

Conflict of Interest

The authors declare no conflict of interest.

Data Availability Statement

The data that support the findings of this study are available from the corresponding author upon reasonable request.

Keywords

amorphous oxide semiconductors (AOS), defects, instabilities, thin-film transistors (TFT)

Received: May 24, 2025
Published online: July 7, 2025

[1] H. Hosono, H. Kumomi, *Amorphous Oxide Semiconductors: IGZO and Related Materials for Display and Memory*, Wiley, Hoboken, New Jersey **2022**.
[2] K. Nomura, H. Ohta, A. Takagi, T. Kamiya, M. Hirano, H. Hosono, *Nature* **2004**, *432*, 488.
[3] A. Nathan, S. Lee, S. Jeon, J. Robertson, *J. Display Technol.* **2014**, *10*, 917.
[4] X. Yu, T. J. Marks, A. Facchetti, *Nat. Mater.* **2016**, *15*, 383.
[5] K. Ide, K. Nomura, H. Hosono, T. Kamiya, *Phys. Status Solidi (a)* **2019**, *216*, 1800372.
[6] T. Kamiya, H. Hosono, *ECS Trans.* **2013**, *54*, 103.
[7] G. W. Mattson, K. T. Vogt, J. F. Wager, M. W. Graham, *J. Appl. Phys.* **2022**, *131*, 105701.
[8] K. Ide, Y. Kikuchi, K. Nomura, M. Kimura, T. Kamiya, H. Hosono, *Appl. Phys. Lett.* **2011**, *99*, 093507.
[9] Y.-S. Shiah, K. Sim, Y. Shi, K. Abe, S. Ueda, M. Sasase, J. Kim, H. Hosono, *Nat. Electron.* **2021**, *4*, 800.
[10] A. Belmonte, H. Oh, N. Rassoul, G. L. Donadio, J. Mitard, H. Dekkers, R. Delhougne, S. Subhechha, A. Chasin, M. J. v. Setten, L. Kljucar, M. Mao, H. Puliyalil, M. Pak, L. Teugels, D. Tsvetanova, K. Banerjee, L. Souriau, Z. Tokei, L. Goux, G. S. Kar, presented at 2020 IEEE Int. Electron Devices Meeting (IEDM) 12–18 Dec. **2020**.
[11] Q. Hu, C. Gu, Q. Li, S. Zhu, S. Liu, Y. Li, L. Zhang, R. Huang, Y. Wu, *Adv. Mater.* **2023**, *35*, 2210554.
[12] S. Yan, Z. Cong, N. Lu, J. Yue, Q. Luo, *Sci. China Inf. Sci.* **2023**, *66*, 200404.
[13] D. Geng, K. Wang, L. Li, K. Myny, A. Nathan, J. Jang, Y. Kuo, M. Liu, *Nat. Electron.* **2023**, *6*, 963.
[14] M. Liu, Z. Li, W. Lu, K. Chen, J. Niu, F. Liao, Z. Wu, C. Lu, W. z. Li, D. Geng, N. Lu, C. Dou, G. Yang, L. Li, M. Liu, presented at 2024 IEEE Symp. on VLSI Technology and Circuits (VLSI Technology and Circuits), **2024**.
[15] F. Liao, Z. Zhu, K. Chen, G. Yang, M. Liu, W. Lu, Z. Wu, J. Niu, C. Lu, B. M. Kang, J. Shi, X. S. Wu, R. Yu, W. Zhang, J. Zhang, G. L. Wang, J. Yue, J. Wang, L. Wang, D. Geng, N. Lu, C. Zhao, A. Nathan, L. Li, M. Liu, presented at 2024 IEEE Int. Electron Devices Meeting (IEDM), **2024**.
[16] S. Fujii, T. F. Lu, K. Ikeda, S. Y. Chang, K. Sakamoto, L. W. Chung, M. Okajima, J. Y. Tsai, T. Kuroda, C. P. Hao, S. Miyano, M. C. Peng, K. Okano, M. Sillero, A. Kajita, C. L. Huang, T. Fujimaki, C. L. Shih, presented at 2024 IEEE Int. Electron Devices Meeting (IEDM), **2024**.
[17] T. Kamiya, H. Hosono, *NPG Asia Mater.* **2010**, *2*, 15.
[18] M. J. Kim, H. J. Park, S. Yoo, M. H. Cho, J. K. Jeong, *IEEE Trans. Electron Devices* **2022**, *69*, 2409.
[19] T. H. Chiang, B. S. Yeh, J. F. Wager, *IEEE Trans. Electron Devices* **2015**, *62*, 3692.
[20] Y. Shi, M. Tsuji, H. Cho, S. Ueda, J. Kim, H. Hosono, *ACS Nano* **2024**, *18*, 9736.
[21] J. H. Jeong, S. W. Seo, D. Kim, S. H. Yoon, S. H. Lee, B. J. Kuh, T. Kim, J. K. Jeong, *Sci. Rep.* **2024**, *14*, 10953.
[22] G. L. Pearson, J. Bardeen, *Phys. Rev.* **1949**, *75*, 865.
[23] P. Kozodoy, H. Xing, S. P. DenBaars, U. K. Mishra, A. Saxler, R. Perrin, S. Elhamri, W. C. Mitchel, *J. Appl. Phys.* **2000**, *87*, 1832.
[24] R. L. Weiher, *J. Appl. Phys.* **1962**, *33*, 2834.
[25] I. Stenger, M.-A. Pinault-Thaury, T. Kociniewski, A. Lusson, E. Chikoidze, F. Jomard, Y. Dumont, J. Chevallier, J. Barjon, *J. Appl. Phys.* **2013**, *114*, 073711.
[26] P. P. Debye, E. M. Conwell, *Phys. Rev.* **1954**, *93*, 693.
[27] H. Cho, M. Tsuji, J. Kim, H. Hosono, presented at Proc. of the Int. Display Workshops (IDW '23), Niigata, Japan, **2023**.
[28] J. Yao, N. Xu, S. Deng, J. Chen, J. She, H. P. D. Shieh, P. T. Liu, Y. P. Huang, *IEEE Trans. Electron Devices* **2011**, *58*, 1121.
[29] N. Nakamura, J. Kim, H. Hosono, *Adv. Electron. Mater.* **2018**, *4*, 1700352.
[30] Y. Shi, Y.-S. Shiah, K. Sim, M. Sasase, J. Kim, H. Hosono, *Appl. Phys. Lett.* **2022**, *121*, 212101.
[31] J. K. Jeong, H. W. Yang, J. H. Jeong, Y.-G. Mo, H. D. Kim, *Appl. Phys. Lett.* **2008**, *93*, 123508.
[32] L.-M. Tang, L.-L. Wang, D. Wang, J.-Z. Liu, K.-Q. Chen, *J. Appl. Phys.* **2010**, *107*, 083704.
[33] T. Kamiya, K. Nomura, H. Hosono, *J. Display Technol.* **2009**, *5*, 462.
[34] S. Ueda, *Appl. Phys. Express* **2018**, *11*, 105701.
[35] S. Ueda, Y. Fujita, Y. Sakuraba, *Phys. Rev. B* **2024**, *109*, 085109.
[36] M. Chen, X. Wang, Y. H. Yu, Z. L. Pei, X. D. Bai, C. Sun, R. F. Huang, L. S. Wen, *Appl. Surf. Sci.* **2000**, *158*, 134.
[37] T. Szörényi, L. D. Laude, I. Bertóti, Z. Kántor, Z. Geretovszky, *J. Appl. Phys.* **1995**, *78*, 6211.
[38] K. Nomura, T. Kamiya, E. Ikenaga, H. Yanagi, K. Kobayashi, H. Hosono, *J. Appl. Phys.* **2011**, *109*, 073726.

[39] J.-C. Dupin, D. Gonbeau, P. Vinatier, A. Levasseur, *Phys. Chem. Chem. Phys.* **2000**, *2*, 1319.
[40] P. T. Hsieh, Y. C. Chen, K. S. Kao, C. M. Wang, *Appl. Phys. A* **2008**, *90*, 317.
[41] W. K. Choi, H. J. Jung, S. K. Koh, *J. Vac. Sci. Technol., A* **1996**, *14*, 359.
[42] K. Xiong, J. Robertson, M. C. Gibson, S. J. Clark, *Appl. Phys. Lett.* **2005**, *87*, 183505.
[43] J. Strand, P. La Torraca, A. Padovani, L. Larcher, A. L. Shluger, *J. Appl. Phys.* **2022**, *131*, 234501.
[44] D. L. Griscom, *J. Non-Cryst. Solids* **1985**, *73*, 51.
[45] H. Hosono, Y. Ikuta, T. Kinoshita, K. Kajihara, M. Hirano, *Phys. Rev. Lett.* **2001**, *87*, 175501.
[46] K. Kajihara, L. Skuja, M. Hirano, H. Hosono, *Phys. Rev. Lett.* **2002**, *89*, 189901.
[47] T. Kamiya, K. Nomura, M. Hirano, H. Hosono, *Phys. Status Solidi c* **2008**, *5*, 3098.
[48] L. S. R. Kumara, K. Ishikawa, K. Ide, H. Hosono, T. Kamiya, O. Sakata, *J. Phys. Chem. C* **2021**, *125*, 13619.
[49] I. Chatratin, F. P. Sabino, P. Reunchan, S. Limpijumnong, J. B. Varley, C. G. Van de Walle, A. Janotti, *Phys. Rev. Mater.* **2019**, *3*, 074604.
[50] A. Walsh, D. O. Scanlon, *Phys. Rev. B* **2013**, *88*, 161201.
[51] J. Lehtomäki, J. Li, P. Rinke, *J. Phys. Commun.* **2020**, *4*, 125001.
[52] S. Lany, A. Zunger, *Phys. Rev. Lett.* **2007**, *98*, 045501.
[53] T. Miyase, K. Watanabe, I. Sakaguchi, N. Ohashi, K. Domen, K. Nomura, H. Hiramatsu, H. Kumomi, H. Hosono, T. Kamiya, *ECS J. Solid State Sci. Technol.* **2014**, *3*, Q3085.
[54] T. Kamiya, K. Nomura, H. Hosono, *J. Disp. Technol.* **2009**, *5*, 468.
[55] H. Hosono, K. Ueda, in *Springer Handbook of Electronic and Photonic Materials*, (Eds: S. Kasap, Ed., P. Capper), Springer International Publishing, Cham **2017**.
[56] H. Hosono, K. Nomura, Y. Ogo, T. Uruga, T. Kamiya, *J. Non-Cryst. Solids* **2008**, *354*, 2796.
[57] H. Tang, K. Ide, H. Hiramatsu, S. Ueda, N. Ohashi, H. Kumomi, H. Hosono, T. Kamiya, *Thin Solid Films* **2016**, *614*, 73.
[58] K. Ide, K. Nomura, H. Hiramatsu, T. Kamiya, H. Hosono, *J. Appl. Phys.* **2012**, *111*, 073513.
[59] A. Yasui, Y. Takagi, T. Osaka, Y. Senba, H. Yamazaki, T. Koyama, H. Yumoto, H. Ohashi, K. Motomura, K. Nakajima, M. Sugahara, N. Kawamura, K. Tamasaku, Y. Tamenori, M. Yabashi, *J. Synchrotron Radiat.* **2023**, *30*, 1013.